RESEARCH ARTICLE | DECEMBER 04 2023

A room temperature exchange bias effect caused by the coexisting martensitic phase structures in Ni₅Mn₃₅Sb₁₂-xGax polycrystalline Heusler alloys ⊘

Fanghua Tian ■ ⑤ ; Tieyan Chang; Qizhong Zhao; Jiale Guo; Long Xian; Kaiyan Cao; Zhiyong Dai ⑥ ; Yin Zhang ⑥ ; Chao Zhou ⑥ ; Sen Yang ■ ⑥

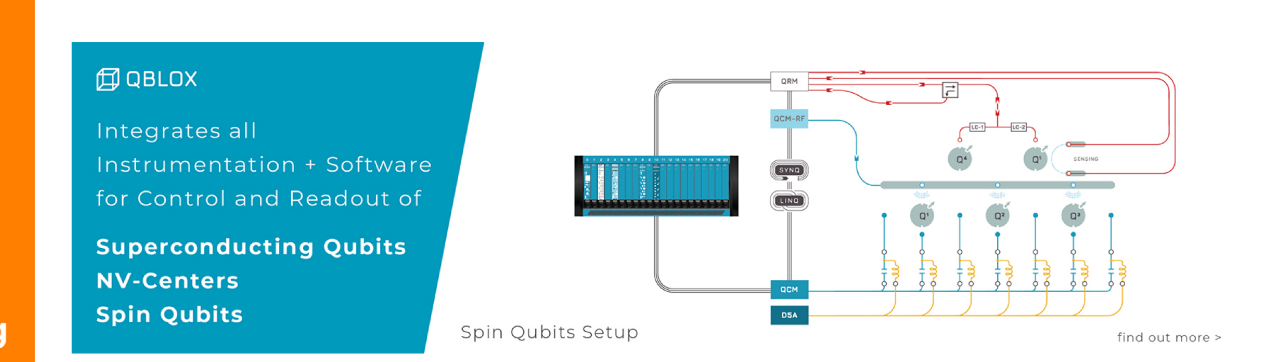


Appl. Phys. Lett. 123, 232402 (2023) https://doi.org/10.1063/5.0178839





CrossMark





A room temperature exchange bias effect caused by the coexisting martensitic phase structures in Ni₅₀Mn₃₈Sb_{12-x}Ga_x polycrystalline Heusler alloys

Cite as: Appl. Phys. Lett. **123**, 232402 (2023); doi: 10.1063/5.0178839 Submitted: 28 September 2023 · Accepted: 18 November 2023 · Published Online: 4 December 2023







Fanghua Tian,^{1,a)} Tieyan Chang,² Qizhong Zhao,¹ Jiale Guo,¹ Long Xian,¹ Kaiyan Cao,¹ Zhiyong Dai,¹ Ain Zhang,¹ Chao Zhou,¹ and Sen Yang^{1,a)}

AFFILIATIONS

¹MOE Key Laboratory for Nonequilibrium Synthesis and Modulation of Condensed Matter, School of Physics, Xi'an Jiaotong University, Xi'an 710049, China

²NSF's ChemMatCARS, The University of Chicago, Lemont, Illinois 60439, USA

ABSTRACT

The exchange bias effect is the physical cornerstone of applications, such as spin valves, ultra-high-density data storage, and magnetic tunnel junctions. This work studied the room temperature exchange bias effect by constructing a $Ni_{50}Mn_{38}Sb_{12-x}Ga_x$ alloy system with coexisting martensitic phase structures. The study found that the exchange bias effect shows a non-monotonic change with the variation of Ga composition at 300 K, and an obvious room temperature exchange bias effect appears in the alloys with coexisting phase structures of 4O and $L1_0$, which is due to the strong exchange coupling between ferromagnetic and antiferromagnetic. Further research on the exchange bias effect and temperature shows that the blocking temperature is 420 K, and the exchange bias can stably exist in a temperature range of \sim 200 K around room temperature. This work provides a method to engineer exchange bias effects at room temperature.

Published under an exclusive license by AIP Publishing. https://doi.org/10.1063/5.0178839

A new exchange anisotropy was first discovered in Co/CoO by Meiklejohn and Bean in 1956, resulting from the exchange interaction between the ferromagnetic (FM) and antiferromagnetic (AFM). Accompanied by anisotropy, the hysteresis loop of a magnetic sample shifts along the magnetic field axis after it cools by an external magnetic field which is known as the exchange bias (EB) effect. 1-3 It has been extensively studied for its potential role in spin valves, ultra-high-density data storage, magnetic tunnel junctions, and spintronic devices. 4-6 So far, this effect has been found in different materials systems, such as FM/AFM core/shell nanoparticles, 7.8 FM/AFM films, 9,10 and materials with phase separation (Heusler alloys and perovskite oxides, etc.), 11,12 in which the FM domains are coupled to AFM domains by exchange interaction.

For ${\rm Ni_2Mn_{1+x}Z_{1-x}}$ (In, Ga, Sb, etc.) Heusler alloy, the magnetic moments for Ni atoms are much smaller than the Mn atoms, so the contribution of the Ni magnetic moments in the total magnetic moments is usually ignored and only the contribution of Mn atoms is considered. ^{13,14} The relation between exchange interaction and Mn–Mn distance (${\rm d_{Mn-Mn}}$) is conformed to the Bethe–Slater curve that describes the relation between the exchange coupling and

interatomic distance. 15,16 When $d_{Mn-Mn} < 2.83 \, \text{Å}$, the interaction is AFM due to the lower energy state of AFM order, and for $d_{\mathrm{Mn-Mn}}$ \geq 2.83 Å, it is FM, that is, in martensite, when d_{Mn-Mn} smaller than 2.83 Å dominates, it exhibits AFM. When d_{Mn-Mn} larger than 2.83 Å dominates, it shows FM. 17-19 The diverse structure of Heusler alloy martensite (tetragonal, monoclinic, orthorhombic, etc.) produces diverse magnetic states, among which the tetragonal phase will enhance AFM.^{20–22} In studying the EB effect of Heusler alloys, cooling field and blocking temperature are important research focuses. On the one hand, zero-field cooling (ZFC) can reduce energy consumption. On the other hand, a higher blocking temperature is more conducive to the practical application of the EB effect. In 2007, Khan et al. used the method of composition control in $\text{Ni}_{50}\text{Mn}_{25+x}\text{Sb}_{25-x}$ and observed that $Ni_{50}Mn_{38.5}Sb_{11.5}$ had an EB effect of 284 Oe when it was cooled under 50 kOe at 5 K;²³ at the same time, Jing et al. also found that an EB effect of 175 Oe at 2 K can be obtained in Ni₅₀Mn₃₆Sn₁₄ after field cooling under 10 kOe.²⁴ Subsequently, in 2011, Wang et al. observed the EB effect after zero-field cooling in the antiferromagnetic spin glass (SG) Ni₅₀Mn₃₇In₁₃ (10 K), which is due to the long-range disordered and short-range ordered ferromagnetism at low temperature. 25 After

^{a)}Authors to whom correspondence should be addressed: tfh2017@xjtu.edu.cn and yangsen@xjtu.edu.cn

this, the EB effect $[1.7 \, \text{kOe}$ at $1.9 \, \text{K},^{26} \, 2.3 \, \text{kOe}$ at $50 \, \text{K},^{27} \, 0.25 \, \text{kOe}$ at $5 \, \text{K},^{28}$ and $1.28 \, \text{kOe}$ at $10 \, \text{K}$ (Ref. 29)] after zero-field cooling was also discovered in many other systems, but the blocking temperature still only increased to about $150 \, \text{K}$.

In this work, the $Ni_{50}Mn_{38}Sb_{12-x}Ga_x$ ($0 \le x \le 12$) polycrystalline alloy system was constructed. When $5 \le x \le 8$, the alloys are coexisting martensitic structures with different magnetic phases (FM and AFM), thus arising the EB effect at room temperature (300 K). The variation of the EB effect with Ga composition (x) was investigated. Experimental results show that with the increasing x, the room temperature EB effect shows a non-monotonic trend of first increasing and then decreasing. In alloys (for example, $Ni_{50}Mn_{38}Sb_5Ga_7$, etc.) with coexisting martensitic phase structures, an optimal EB effect of 175 Oe was obtained at room temperature. At the same time, the changing trend of the EB effect with temperature was studied, and the EB effect can exist in a wide temperature range of about 200 K near room temperature. This result provides a method for designing and preparing materials with an EB effect at room temperature.

The Ni₅₀Mn₃₈Sb_{12-x}Ga_x ($0 \le x \le 12$) alloy system was prepared according to the stoichiometric ratio by arc melting, the ingots were smelted five times, and the purity of all raw materials was 99.9%. To achieve high composition homogeneity, the samples were wrapped in silica tubes and vacuum annealed at 1173 K for 24 h. The differential scanning calorimetry (DSC) was used to determine the martensitic transition temperature. X-ray diffraction (XRD, Bruker D8 Advance x-ray diffractometer, Germany, Cu K α , $\lambda = 0.154\,18\,\mathrm{nm}$) was used to

investigate the crystalline nature of alloys. The sample was also sealed in Kapton capillaries for $in\ situ\ HR-XRD$ measurements with $\lambda=0.4142\,\mbox{\normalfont\AA}$ at beamline 11-BM-B at the Advanced Photon Source, Argonne National Laboratory. The magnetic properties, including magnetic hysteresis (MH) loops, magnetization temperature (MT) curves, and AC susceptibility, were measured using a superconducting quantum interference device (SQUID) magnetometer (Quantum Design, MPMS-XL-5).

The composition-temperature phase diagram of Ni₅₀Mn₃₈Sb_{12-x}Ga_x $(0 \le x \le 12)$ is shown in Fig. 1(a). DSC [Fig. 1(b)] and XRD [Fig. 1(c)] data determine the entire phase diagram and coexisting phase structure boundary. Strong endothermic and exothermic effects often accompany the first-order phase transformation in alloys, which can be characterized through DSC. The temperatures at which martensite transformation begins, the temperature at which martensite transformation ends, the temperature at which austenite transformation begins, and the temperature at which austenite transformation ends are usually marked as M_S , M_F , A_S , and A_F , respectively. As shown in Fig. 1(b), a set of obvious endothermic and exothermic peaks appear in the DSC analysis spectrum when x = 0, corresponding to martensite phase transformation and inverse martensitic phase transformation. They are starting and ending temperatures. M_S , M_E , A_S , and A_E are 383, 345, 399, and 354 K, respectively, and the thermal hysteresis is about 15 K. Thermal hysteresis is an inherent feature of first-order phase transitions. 30 As the x increases, when x = 7, the martensitic transformation temperature of

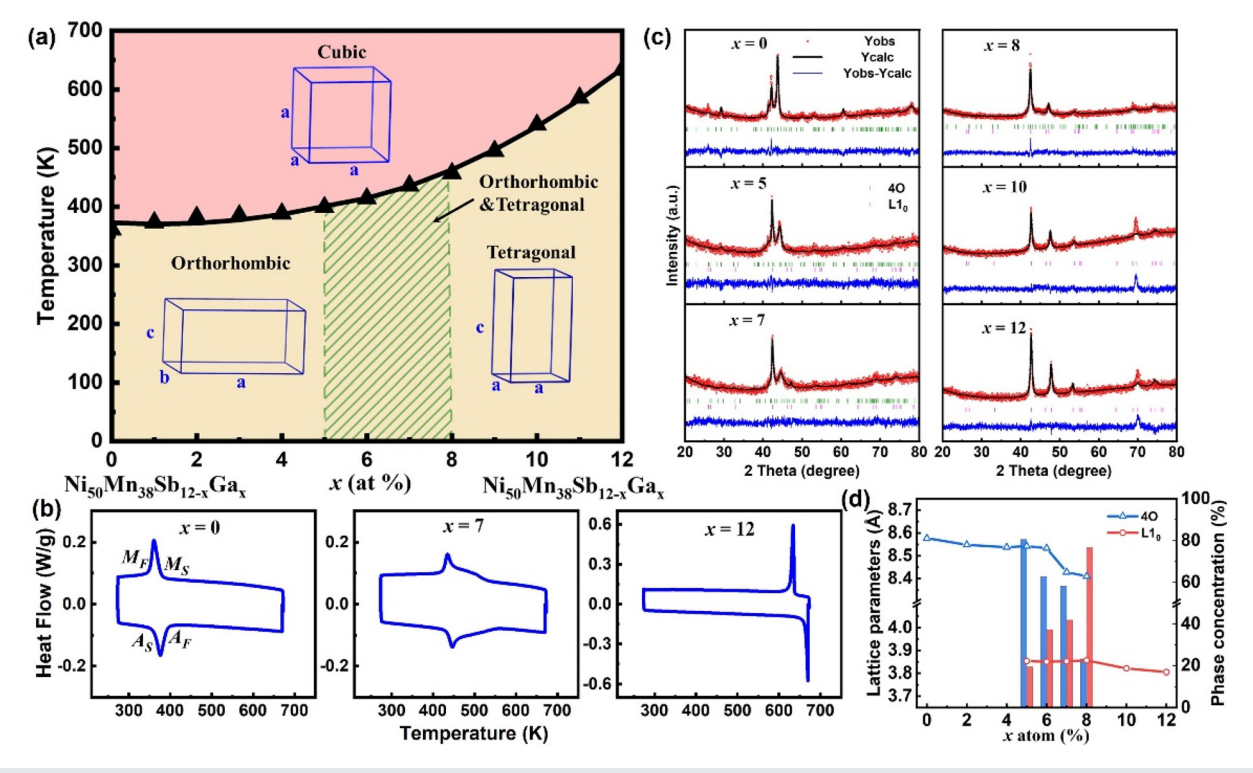


FIG. 1. (a) Phase diagram of $Ni_{50}Mn_{38}Sb_{12-x}Ga_x$ ($0 \le x \le 12$). (b) DSC curves of for $Ni_{50}Mn_{38}Sb_{12-x}Ga_x$ alloys (x = 0, 7, and 12). (c) Room temperature XRD patterns for $Ni_{50}Mn_{38}Sb_{12-x}Ga_x$ alloys (x = 0, 5, 7, 8, 10, and 12). (d) The lattice parameters and phase proportion dependence on x of $Ni_{50}Mn_{38}Sb_{12-x}Ga_x$ ($0 \le x \le 12$) alloys, the blue column represents the proportion of 40, and the red column represents the proportion of $L1_0$.

Ni₅₀Mn₃₈Sb₅Ga₇ alloy moves to high temperature. With the further rise of x, the M_S of $Ni_{50}Mn_{38}Ga_{12}$ has been increased to 641 K. It can also be observed from the DSC that as the proportion of Sb and Ga change, the intensity and shape of the endothermic and exothermic peaks also change. The endothermic peak intensity of Ni₅₀Mn₃₈Sb₅Ga₇ is the lowest, and the shape is not as sharp as the endothermic peaks of Ni₅₀Mn₃₈Ga₁₂ and Ni₅₀Mn₃₈Sb₁₂, there is also a small step around the endothermic and exothermic peaks. This phenomenon is because the structure of Ni₅₀Mn₃₈Ga₁₂ and Ni₅₀Mn₃₈Sb₁₂ is a single martensite phase, and strong adsorption occurs during the martensitic phase transformation process. However, the martensitic phase of Ni₅₀Mn₃₈Sb₅Ga₇ is a two-phase coexisting martensitic phase with a broad phase transformation temperature range and relatively small heat absorption and generation. As shown in Fig. 1(c), It can be seen from the Rietveld refinement results of the XRD pattern that when $x \le 4$, The XRD diffraction peak shows the obvious characteristic peaks (200), (102), and (221) of four-layer orthorhombic martensite (4O). 31,32 The martensitic structure is a pure 4O phase. In contrast to this, when x > 8, the characteristic peaks of the XRD diffraction peaks are (112), (200), (202), and (440), which belong to the standard non-modulated tetragonal martensite (L1₀). The structure becomes pure L1₀ phase. When $5 \le x \le 8$, it is the coexistence martensitic phase of 4O and L1₀ in the middle compositions. As shown in Fig. 1(d), the proportion of the 4O phase decreases from 80% to 23%, and L1₀ increases from 20% to 77% correspondingly. The change in proportion changes the exchange interaction between systems and, thus, causes the variation of EB. Meanwhile, the lattice parameters of 4O and L10 are obtained from the refinement results. The lattice parameters both decrease with increased x. As shown in Fig. S1, for $Ni_{50}Mn_{38}Sb_{12-x}Ga_x$ (0 $\leq x \leq$ 12) alloy, the grain size increases with increased x. When x=0 and x=12, the grain sizes of ferromagnetic $Ni_{50}Mn_{38}Sb_{12}$ alloy and antiferromagnetic $Ni_{50}Mn_{38}Ga_{12}$ alloy are 80 and 300 μ m, respectively.

Figure 2 shows MH loops at 300 K of the Ni₅₀Mn₃₈Sb_{12-x}Ga_x (0 < x < 12) after zero-field cooling from 400 K, and the inset is the enlarged central region of the loops. The exchange field (H_{EB}) is defined as $H_{EB} = (H_L + H_R)/2$, where H_L and H_R are the left and right coercive fields, respectively. When x = 0, the MH loop shows FM, as xincreased to 12, the MH loop shows AFM. As shown in the inset of Figs. 2(a) and 2(e), the enlarged MH loops for x = 0 and x = 12 do not shift with the magnetic field axis, and no EB effect exists. However, for the coexisting phase structure alloys, the MH loops move right along the x axis, showing an obvious EB effect. Similar behaviors were observed for FeF₂/Fe and La_{0.5}Sr_{0.5}Mn_{0.8}Co_{0.2}O₃ ceramics systems exhibiting a positive EB effect.^{35,36} The positive EB effect is due to the AFM exchange interaction at the AFM/FM interface³⁵ exchange interaction at the interface causes the AFM interfacial spin coupling to the FM interfacial spin. A microscopic torque exerted by the AFM pinning force on the FM layer leads to the unidirectional anisotropy, which causes the MH loops to shift. Thus, when the exchange interaction is AFM, an extra positive measuring field is required to overcome the interface AFM unidirectional anisotropy, thus causing the positive EB effect. Figure 2(f) shows the relationship between the H_{EB} and x, the H_{EB} first increases, and then decreases as the increasing x. The optimal EB effect $H_{EB} = 175 \,\text{Oe}$ appears in Ni₅₀Mn₃₈Sb₅Ga₇ alloys. Hence, H_{EB} is sensitive to the structure. Since the atomic radius of Sb is larger than Ga, when the ratio of Sb and Ga changes, the structure changes from 4O to L10 and 4O and then all change to L10, resulting in a difference in the Mn-Mn distance.

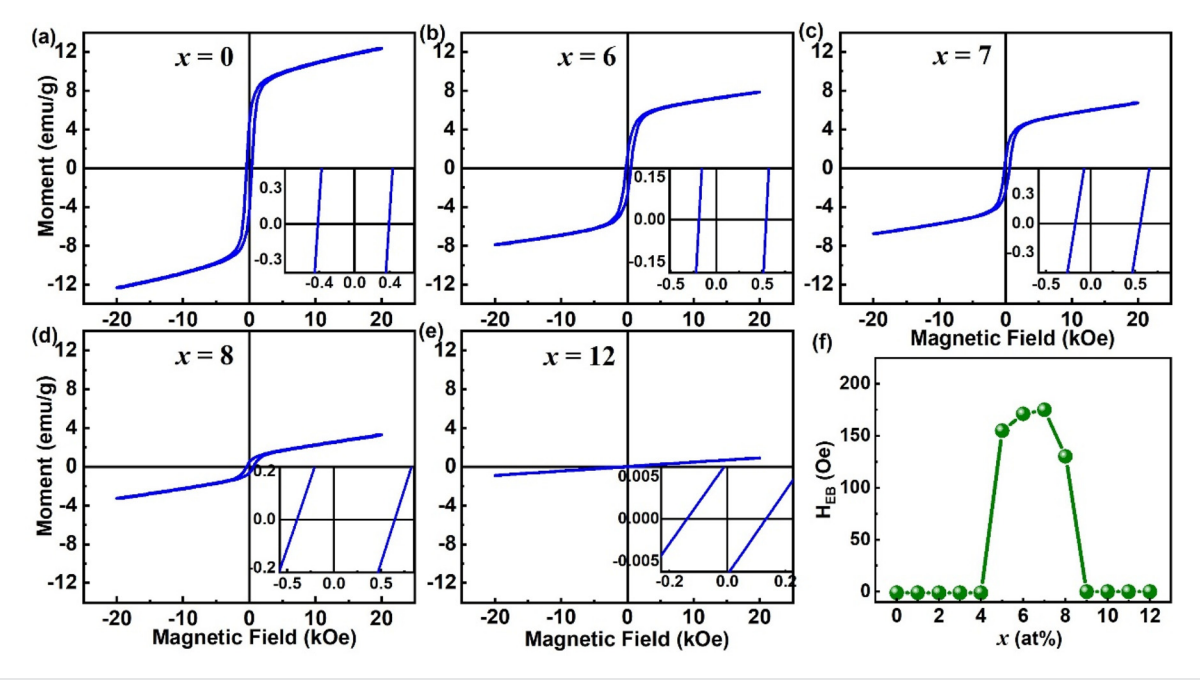


FIG. 2. Magnetization hysteresis loops of $Ni_{50}Mn_{38}Sb_{12-x}Ga_x$ alloys ($0 \le x \le 12$): (a) x = 0, (b) x = 6, (c) x = 7, (d) x = 8, and (e) x = 12. Inset: enlarged view of the central region of the loops. (f) H_{EB} dependent on the x of $Ni_{50}Mn_{38}Sb_{12-x}Ga_x$ measured at 20 kOe after ZFC.

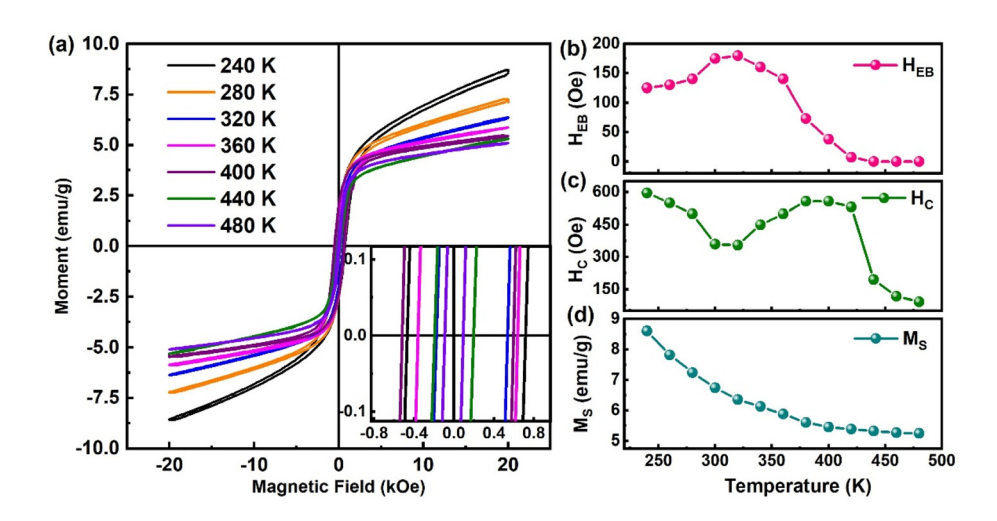


FIG. 3. (a) Magnetization hysteresis loops of Ni $_{50}$ Mn $_{38}$ Sb $_{5}$ Ga $_{7}$ dependent on the temperature. Inset: enlarged view of the central region of loops. (b) H $_{EB}$ dependent on the temperature of Ni $_{50}$ Mn $_{38}$ Sb $_{5}$ Ga $_{7}$ measured at 20 kOe after ZFC. (c) H $_{C}$ dependent on the temperature of Ni $_{50}$ Mn $_{38}$ Sb $_{5}$ Ga $_{7}$. (d) M $_{8}$ dependent on the temperature of Ni $_{50}$ Mn $_{38}$ Sb $_{5}$ Ga $_{7}$.

The magnetism of the alloy changes from FM to the coexistence of FM and AFM which has a strong exchange interaction and finally turns to main AFM.

As shown in Fig. 3(a), the changing trend of the EB effect with temperature was further studied by the MH loops at different temperatures (240-480 K) after zero-field cooling, the MH loops at 240-360 K are tested after zero-field cooling from 400 K and at 320-480 K are tested after zero-field cooling from 500 K. All M-H loops are almost identical in shape. From the enlarged MH curves in the inset Fig. 3(a), there is a noticeable shift in the magnetic field axis below 420 K. Figure 4(b) shows the relationship between H_{EB} and temperature, H_{EB} first increases and gets a peak at 320 K with increasing temperature. As temperatures further rise, the H_{EB} begins to decrease and be zero above 420 K, which is defined as the blocking temperature (T_B). This is mainly affected by the temperature dependence of AFM anisotropy and thermal disturbances. Figure 3(c) shows the changes in coercive force with temperature. The H_C is defined as $H_C = (H_R - H_L)/2$. It can be found that H_C first decreases and then increases as the temperature increases, exhibiting a valley around 320 K. From the previous research, the H_C in the FM/AFM system is attributed to the part of AFM with low anisotropy, which can be dragged by the FM part, and the EB is attributed to the part of AFM with high anisotropy which cannot be dragged by the FM part. 39-41 The AFM anisotropy is high at the temperature where the AFM cannot be dragged easier by the FM, which causes a minimum of H_C and a maximum of H_{EB}. This phenomenon is identical to some previous research on Heusler alloys. 42,43 With a further temperature increase, the H_C peaks at T_B and then begins to decrease. That is because the AFM anisotropy decreases as temperature approaches T_B. Above T_B, AFM can no longer hinder the FM rotation. ^{39–43} As a result, the Hc reaches its maximum value, and H_{EB} reduces to zero at higher temperatures. At the same time, it can also be observed that the saturation magnetization (M_s) gradually increases as the temperature decreases, from 5.2 emu g⁻¹ at 480 K to 8.6 emu g⁻¹ at 240 K [Fig. 3(d)]. The above-mentioned results show this EB effect caused by the coexisting phase structure can exist in a wide temperature range (240-420 K). The EB effect after different field cooling at 300 K has been tested and shown in Fig. S2. With the increasing cooling field, the value of H_{EB} decreases and finally transforms to a negative value. This is owing to the increased FM cluster at the interface with the increasing cooling field and exchange

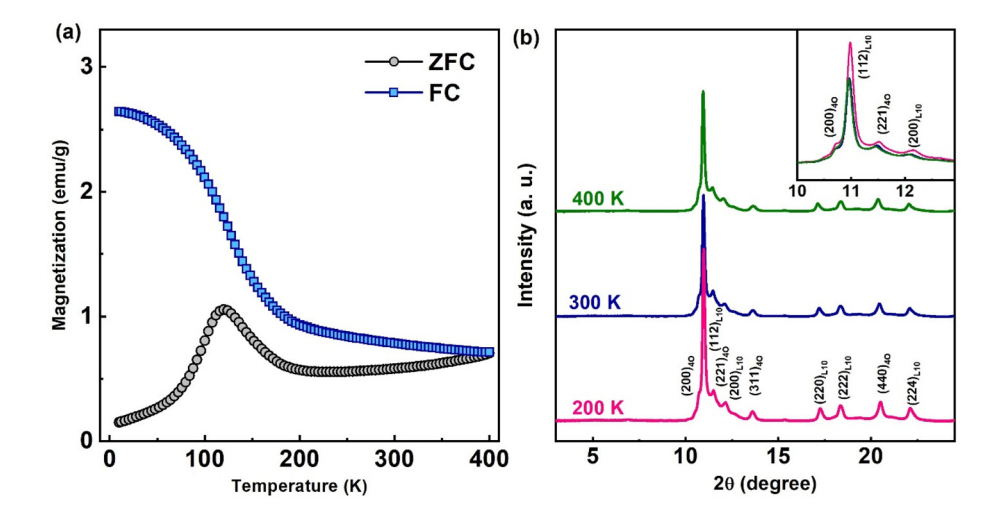


FIG. 4. (a) The magnetization temperature dependence curves measured at 200 Oe with sequences of ZFC and FC for Ni $_{50}$ Mn $_{38}$ Sb $_{5}$ Ga $_{7}$. (b) XRD profiles dependent on temperatures (400, 300, and 200 K). Inset: the enlarged peak of XRD within 2θ range of 10–13.

interaction, thus turning from AFM to FM.³⁷ Then, the MH loops shift to the left along the magnetic field axis offsetting the origin center.

Figure 4 shows the MT curves of Ni₅₀Mn₃₈Sb₅Ga₇ under zerofield cooling (ZFC) and field cooling (FC) conditions. If ZFC curve is cooling the sample from 400 K to 10 K without an external field, then the temperature is raised to 400 K under an external magnetic field (200 Oe), the change in the magnetization of the sample during the heating process is recorded, FC refers to the process of cooling and testing with an external magnetic field. It can be seen that the ZFC and FC curves do not overlap, and the magnetization of ZFC is significantly lower than the FC. The splitting between the ZFC and FC curves increases with decreasing temperature, indicating irreversible magnetization behavior in the alloy, i.e., FM and AFM interactions. This caused the EB effect near room temperature. With a further decrease in temperature, the splitting becomes more pronounced. It is worth noting that in the ZFC curve there is a peak at temperature 125 K (T_p), which is usually considered to indicate the critical temperature of spin glass (SG) or superparamagnetic state (SPM). In general, the MT behaviors of the SG and the SPM systems at lower temperatures are similar under ZFC. However, for the FC curves, the magnetization increases monotonically in SPM systems as the temperature decreases. Rather, the magnetization of SG systems tends to saturate with the decreasing temperature.44 To confirm the existence of SG, we also performed AC susceptibility measurements. Figure S3 shows the temperature dependence of the real part of the AC susceptibility (χ') at different frequency values. It can be seen that each curve has a distinct peak. This peak shifts toward higher temperatures with increasing frequency, which is a typical feature of the spin glass state. 11 The high-resolution XRD patterns of Ni₅₀Mn₃₈Sb₅Ga₇ in the temperatures of 400, 300, and 200 K, shown in Fig. 4(b), can be observed that all the XRD at different temperatures have characteristic peaks of 4O and L1₀. Among them, characteristic peaks, such as (200), (221), (311), and (440) belong to 4O, and characteristic peaks, such as (112), (200), (220), (222), and (224), belong to L1₀. At the same time, the increasing shift in the position of the Bragg peak toward the higher 2θ side with decreasing temperature, as shown in the inset in Fig. 4(b), is apparently due to the usual thermal expansion behavior, and the unit cell parameters become smaller.

In summary, we construct a $Ni_{50}Mn_{38}Sb_{12-x}Ga_x$ ($0 \le x \le 12$) alloy phase diagram through $Ni_{50}Mn_{38}Sb_{12}$ with an FM orthorhombic martensitic structure and $Ni_{50}Mn_{38}Ga_{12}$ with an AFM tetragonal martensitic structure. The $Ni_{50}Mn_{38}Sb_{12-x}Ga_x$ ($5 \le x \le 8$) with 4O and $L1_0$ coexisting martensitic phase structures have FM and AFM magnetic phases. The AFM exchange coupling between the FM and AFM phases induces an EB effect at room temperature. For example, the $Ni_{50}Mn_{38}Sb_5Ga_7$ alloy has a H_{EB} of 175 Oe. Further research found that this EB effect can be observed in a wide temperature range from 240 to 420 K. This work indicates that we can obtain the EB effect at room temperature by constructing alloys with coexisting martensitic phase structures, which not only enriches the theoretical research on EB effect but will also benefit practical applications of this material.

See the supplementary material for the additional tests for the grain size of alloys (Fig. S1), MH loops after cooling under different fields (Fig. S2), and AC susceptibility for Ni₅₀Mn₃₈Sb₅Ga₇ alloy (Fig. S3).

This work was financially supported by the National Key Research and Development Program of China (No. 2021YFB3501401), the

National Natural Science Foundation of China (Grant Nos. 51601140 and 52301250), the Key Scientific and Technological Innovation Team of Shaanxi Province (No. 2020TD001), and the Innovation Capability Support Program of Shaanxi (Nos. 2018PT-28 and 2017KTPT-04). NSF's ChemMatCARS was supported by the Divisions of Chemistry (CHE) and Materials Research (DMR), the National Science Foundation, under NSF/CHE-1834750. Use of the Advanced Photon Source, an Office of Science User Facility operated for the U.S. Department of Energy (DOE) Office of Science by Argonne National Laboratory, was supported by U.S. DOE under Contract No. DE-AC02-06CH11357.

AUTHOR DECLARATIONS

Conflict of Interest

The authors have no conflicts to disclose.

Author Contributions

Fanghua Tian: Conceptualization (lead); Data curation (equal); Formal analysis (lead); Investigation (lead); Writing – original draft (lead); Writing – review & editing (lead). Sen Yang: Funding acquisition (lead); Supervision (lead); Writing – review & editing (equal). Tieyan Chang: Data curation (equal); Formal analysis (equal); Investigation (lead); Methodology (equal). Qizhong Zhao: Data curation (equal); Formal analysis (equal); Investigation (equal); Writing – original draft (supporting); Writing – review & editing (equal). Jiale Guo: Data curation (equal); Investigation (equal). Long Xian: Data curation (supporting); Investigation (equal). Kaiyan Cao: Data curation (equal); Investigation (supporting). Zhiyong Dai: Formal analysis (supporting); Investigation (supporting). Yin Zhang: Formal analysis (supporting); Writing – review & editing (supporting). Chao Zhou: Writing – review & editing (supporting).

DATA AVAILABILITY

The data that support the findings of this study are available from the corresponding author upon reasonable request.

REFERENCES

- ¹W. H. Meiklejohn and C. P. Bean, "New magnetic anisotropy," Phys. Rev. 102, 1413 (1956).
- ²B. Liu, B. Wang, T. Nie, Y. Xie, H. Yang, G. Li, J. Pan, and R.-W. Li, "Effect of isothermal crystallization in antiferromagnetic IrMn on the formation of spontaneous exchange bias," Appl. Phys. Lett. 118, 252404 (2021).
- ³A. K. Nayak, M. Nicklas, S. Chadov, P. Khuntia, C. Shekhar, A. Kalache, M. Baenitz, Y. Skourski, V. K. Guduru, A. Puri, U. Zeitler, J. M. D. Coey, and C. Felser, "Design of compensated ferrimagnetic Heusler alloys for giant tunable exchange bias," Nat. Mater. 14, 679–684 (2015).
- ⁴V. Skumryev, S. Stoyanov, Y. Zhang, G. Hadjipanayis, D. Givord, and J. Nogués, "Beating the superparamagnetic limit with exchange bias," Nature 423, 850 (2003).
- ⁵S. Fukami, C. Zhang, S. DuttaGupta, A. Kurenkov, and H. Ohno, "Magnetization switching by spin-orbit torque in an antiferromagnet-ferromagnet bilayer system," Nat. Mater. 15, 535 (2016).
- ⁶J. Barker, B. Craig, R. Lamberton, A. Johnston, R. W. Chantrell, and O. Heinonen, "A model of the exchange bias setting process in magnetic read sensors," Appl. Phys. Lett. 95, 022504 (2009).
- ⁷H. Khurshid, M.-H. Phan, P. Mukherjee, and H. Srikanth, "Tuning exchange bias in Fe/γ-Fe₂O₃ core-shell nanoparticles: Impacts of interface and surface spins," Appl. Phys. Lett. **104**(7), 072407 (2014).

- ⁸B. Muzzi, M. Albino, M. Petrecca, C. Innocenti, C. d. J. Fernández, G. Bertoni, C. Marquina, M. R. Ibarra, and C. Sangregorio, "3d metal doping of core@shell wüstite@ferrite nanoparticles as a promising route toward room temperature exchange bias magnets," Small 18, 2107426 (2022).
- ⁹S. Hu, K. Pei, B. Wang, W. Xia, H. Yang, Q. Zhan, X. Li, X. Liu, and R.-W. Li, "Direct imaging of cross-sectional magnetization reversal in an exchangebiased CoFeB/IrMn bilayer," Phys. Rev. B **97**, 054422 (2018).
- ¹⁰F. Tian, Y. Li, Q. Zhao, K. Cao, D. Wang, Z. Dai, Z. Yu, X. Ke, Y. Zhang, C. Zhou, W. Zuo, S. Yang, and X. Song, "Giant exchange bias induced via tuning interfacial spins in polycrystalline Fe₃O₄/CoO bilayers," Phys. Chem. Chem. Phys. 23, 4805 (2021).
- ¹¹F. Tian, X. Ke, K. Cao, D. Wang, Q. Zhao, J. Li, Z. Dai, D. Wang, Y. Zhang, C. Zhou, Y. Wang, W. Zuo, M. Fang, and S. Yang, "Tailoring exchange bias in reentrant spin glass by ferromagnetic cluster size engineering," APL Mater. 9, 011104 (2021).
- ¹²D. Deng, J. Zheng, D. Yu, B. Wang, D. Sun, M. Avdeev, Z. Feng, C. Jing, B. Lu, W. Ren, S. Cao, and J. Zhang, "Cooling field tuned magnetic phase transition and exchange bias-like effect in Y_{0.9}Pr_{0.1}CrO₃," Appl. Phys. Lett. **107**, 102404 (2015).
- ¹³ A. Ayuela, J. Enkovaara, K. Ullakko, and R. M. Nieminen, "Structural properties of magnetic Heusler alloys," J. Phys.: Condens. Matter 11, 2017–2026 (1999).
- ¹⁴E. Simon, J. G. Vida, S. Khmelevskyi, and L. Szunyogh, "Magnetism of ordered and disordered Ni₂MnAl full Heusler compounds," Phys. Rev. B **92**, 054438 (2015).
- 15 R. Cardias, A. Szilva, A. Bergman, I. Di Marco, M. I. Katsnelson, A. I. Lichtenstein, L. Nordström, A. B. Klautau, O. Eriksson, and Y. O. Kvashnin, "The Bethe-Slater curve revisited; new insights from electronic structure theory," Sci. Rep. 7, 4058 (2017).
- 16Y. Mokrousov, G. Bihlmayer, S. Blügel, and S. Heinze, "Magnetic order and exchange interactions in monoatomic 3d transition-metal chains," Phys. Rev. B 75, 104413 (2007).
- 17 L. Jia, J. Shen, M. Li, X. Wang, L. Ma, C. Zhen, D. Hou, E. Liu, W. Wang, and G. Wu, "Tuning antiferromagnetic exchange interaction for spontaneous exchange bias in MnNiSnSi system," APL Mater. 5, 126105 (2017).
- 18 V. S. Bai and T. Rajasekharan, "Evidence of a critical Mn-Mn distance for the onset of ferromagnetism in NiAs type compounds," J. Magn. Magn. Mater. 42(2), 198–200 (1984).
- ¹⁹X. Wang, M. Li, J. Li, J. Deng, Y. Wang, L. Ma, D. Zhao, C. Zhen, D. Hou, E. Liu, W. Wang, and G. Wu, "Design of Mn–Mn distance for tunable spontaneous exchange bias in Heusler alloys," Intermetallics 132, 107170 (2021).
- ²⁰J. Wang, C. Jiang, R. Techapiesancharoenkij, D. Bono, S. M. Allen, and R. C. O'Handley, "Microstructure and magnetic properties of melt spinning Ni-Mn-Ga," Intermetallics 32, 151–155 (2013).
- ²¹E. Şaşıoğlu, L. M. Sandratskii, and P. Bruno, "Pressure dependence of the Curie temperature in Ni₂MnSn Heusler alloy: A first-principles study," Phys. Rev. B 71, 214412 (2005).
- ²²P. Entel, M. E. Gruner, S. Fähler, M. Acet, A. Cahır, R. Arroyave, S. Sahoo, T. C. Duong, A. Talapatra, L. Sandratskii, S. Mankowsky, T. Gottschall, O. Gutfleisch, P. Lazpita, V. A. Chernenko, J. M. Barandiaran, V. V. Sokolovskiy, and V. D. Buchelnikov, "Probing structural and magnetic instabilities and hysteresis in Heuslers by density functional theory calculations," Phys. Status Solidi B 255, 1700296 (2018).
- ²³M. Khan, I. Dubenko, S. Stadler, and N. Ali, "Exchange bias behavior in Ni-Mn-Sb Heusler alloys," Appl. Phys. Lett. **91**, 072510 (2007).
- ²⁴Z. Li, C. Jing, J. Chen, S. Yuan, S. Cao, and J. Zhang, "Observation of exchange bias in the martensitic state of Ni₅₀Mn₃₆Sn₁₄ Heusler alloy," Appl. Phys. Lett. 91, 112505 (2007).
- ²⁵B. M. Wang, Y. Liu, P. Ren, B. Xia, K. B. Ruan, J. B. Yi, J. Ding, X. G. Li, and L. Wang, "Large exchange bias after zero-field cooling from an unmagnetized state," Phys. Rev. Lett. 106, 077203 (2011).

- ²⁶A. K. Nayak, M. Nicklas, S. Chadov, C. Shekhar, Y. Skourski, J. Winterlik, and C. Felser, "Large zero-field cooled exchange-bias in bulk Mn₂PtGa," Phys. Rev. Lett. 110, 127204 (2013).
- ²⁷L. G. Wang, C. M. Zhu, Z. M. Tian, H. Luo, D. L. G. C. Bao, and S. L. Yuan, "Negative magnetization and zero-field cooled exchange bias effect in Co_{0.8}Cu_{0.2}Cr₂O₄ ceramics," Appl. Phys. Lett. 107, 152406 (2015).
- ²⁸A. N. Dobrynin, P. Warin, A. Vorobiev, and D. Givord, "On the origin of positive exchange bias and coercivity enhancement in proximity to the blocking temperature," J. Magn. Magn. Mater. 520, 166707 (2021).
- ²⁹F. Tian, Y. Li, Q. Zhao, M. Fang, R. Zhang, Z. Dai, Z. Yu, X. Ke, Y. Zhang, C. Zhou, and S. Yang, "Maximizing zero-field-cooled exchange bias in crystallized Co@CoO nanocluster assembled thin film by varying film thickness," J. Phys. Chem. C 125, 7337–7342 (2021).
- ³⁰C. Zhou, T. Chang, Z. Dai, Y. Chen, C. Guo, Y. Matsushita, X. Ke, A. Murtaza, Y. Zhang, F. Tian, W. Zuo, Y. Chen, S. Yang, and X. Ren, "Unified understanding of the first-order nature of the transition in TbCo₂," Phys. Rev. B 106(6), 064409 (2022).
- ³¹W. J. Feng, L. Zuo, Y. B. Li, Y. D. Wang, M. Gao, and G. L. Fang, "Abnormal e/a-dependence of TM and large inverse magnetocaloric effect in Ni_{49-x}Cu_xMn₃₉Sb₁₂ alloys," Mater. Sci. Eng., B **176**, 621–625 (2011).
- ³²P. J. Brown, A. P. Gandy, K. Ishida, R. Kainuma, T. Kanomata, K.-U. Neumann, K. Oikawa, B. Ouladdiaf, and K. R. A. Ziebeck, "The magnetic and structural properties of the magnetic shape memory compound Ni₂Mn_{1.44}Sn_{0.56}," J. Phys.: Condens. Matter 18, 2249–2259 (2006).
- ³³L. Righi, F. Albertini, L. Pareti, A. Paoluzi, and G. Calestani, "Commensurate and incommensurate '5M' modulated crystal structures in Ni–Mn–Ga martensitic phases," Acta Mater. 55, 5237–5245 (2007).
- 34H. Zheng, W. Wang, S. Xue, Q. Zhai, J. Frenzel, and Z. Luo, "Composition-dependent crystal structure and martensitic transformation in Heusler Ni–Mn–Sn alloys," Acta Mater. 61, 4648–4656 (2013).
- 35J. Nogues, D. Lederman, T. J. Moran, and I. K. Schuller, "Positive exchange bias in FeF₂-Fe bilayers," Phys. Rev. Lett. 76, 4624–4627 (1996).
- ³⁶C. Shang, S. Guo, R. Wang, Z. Sun, H. Xiao, L. Xu, C. Yang, and Z. Xia, "Positive to negative zero-field cooled exchange bias in La_{0.5}Sr_{0.5}Mn_{0.8}Co_{0.2}O₃ ceramics," Sci. Rep. 6(1), 25703 (2016).
- ³⁷J. Krishna Murthy and P. S. Anil Kumar, "Interface-induced spontaneous positive and conventional negative exchange bias effects in bilayer La_{0.7}Sr_{0.3}MnO₃/Eu_{0.45}Sr_{0.55}MnO₃ heterostructures," Sci. Rep. 7, 6919 (2017).
- 38 S. K. Mishra, F. Radu, H. A. Durr, and W. Eberhardt, "Training-induced positive exchange bias in NiFe/IrMn bilayers," Phys. Rev. Lett. 102, 177208 (2009).
- 39A. G. Silva, K. L. Salcedo Rodriguez, C. P. Contreras Medrano, G. S. G. Lourenco, M. Boldrin, E. Baggio-Saitovitch, and L. Bufaical, "Griffiths phase and spontaneous exchange bias in La_{1.5}Sr_{0.5}CoMn_{0.5}Fe_{0.5}O₆," J. Phys.: Condens. Matter 33, 065804 (2021).
- ⁴⁰J. Nogues and I. K. Schuller, "Exchange bias," J. Magn. Magn. Mater. 192, 203–232 (1999).
- ⁴¹M. Ali, C. H. Marrows, M. Al-Jawad, B. J. Hickey, A. Misra, U. Nowak, and K. D. Usadel, "Antiferromagnetic layer thickness dependence of the IrMn/Co exchange-bias system," Phys. Rev. B 68, 214420 (2003).
- ⁴²P. Liao, C. Jing, X. L. Wang, Y. J. Yang, D. Zheng, Z. Li, B. J. Kang, D. M. Deng, S. X. Cao, J. C. Zhang, and B. Lu, "Strongly enhanced antiferromagnetism and giant spontaneous exchange bias in Ni₅₀Mn₃₆Co₄Sn₁₀ Heusler alloy," Appl. Phys. Lett. **104**, 092410 (2014).
- ⁴³R. Vishnoi and D. Kaur, "Exchange bias behaviour in magnetron sputtered Ni_{49.8}Mn_{36.1}Sn_{13.9} ferromagnetic shape memory alloy thin film," J. Alloy. Compd. **509**, 2833–2837 (2011).
- ⁴⁴X. Chen, S. Bedanta, O. Petracic, W. Kleemann, S. Sahoo, S. Cardoso, and P. P. Freitas, "Superparamagnetism versus superspin glass behavior in dilute magnetic nanoparticle systems," Phys. Rev. B 72, 214436 (2005).